New adaptive droop control with combined line impedance estimation method for parallel inverters

- **Le Minh Phuong –** ***E-mail: lmphuong@hcmut.edu.vn***
- **Hoang Vo Duc Duy**
- **Pham Thi Xuan Hoa**
- **Nguyen Minh Huy**

Ho Chi Minh City University of Technology, VNU-HCM

(Manuscript Received on Octorber 04th, 2016, Manuscript Revised December 08th, 2016)

ABSTRACT

This paper presents a new load sharing control between paralleled three-phase inverters in an islanded-microgrid based on the line impedance estimation online by the use of the Kalman filter. We can solve the mismatch of power sharing when the line impedance changes due to the temperature and frequency, significant differences of line parameters and requirements of Plug-and-Play mode of inverters connected to the microgrid. Moreover, the paper also presents a new Droop control method working with the line impedance which is different from the Droop traditional algorithm when the line impedance is assumed pure resistance R or pure inductance X. In the paper, the line impedance estimation for parallel inverters uses the least squares method combined with Kalman filter. In addition, secondary control loops are designed to restore the voltage amplitude and frequency of the microgrid by using a combined nominal value SOGI-PLL with generalized integral block and phase lock loop to exactly monitor the voltage magnitude and frequency phase at common PCC. Control model has been simulated in Matlab/Simulink with three voltage source inverters connected in parallel for different ratios of the power sharing. The simulation results have shown the accuracy of the proposed control method. Therefore, the proposed adaptive droop control method based on line impedance estimation can be an alternative one for load sharing control in islanded microgrids.

Keywords: *Droop control, microgrid, impedance estimation, Kalman filter.*

1. INTRODUCTION

With the expansion of the electrical power grid, the conventional power system has become increasingly vulnerable to cope with the reliability requirements and the diverse demand of power users. Moreover, distributed generation (DG) has appeared to advantages such as pollution reduction, high-energy utilization rate, flexible installation location, and

low-power transmission losses [1]-[2]. DG units have also a higher degree of controllability and operability compared to the conventional generators which will allow microgrids to play a major and critical role in maintaining the reliability and stability of electric networks [3]-[6]. Therefore, microgrids will gradually become a strong and effective support for the main power grid and a potential one for the future trends of power systems [7].

In fact, the renewable energy resources such as the wind, solar and tidal energy are connected to the conventional grid through the converter today and the microgrids are formed before they are connected to the grid [8]-[12]. In the grid-connected mode, the DG units are often controlled as grid-following. The most adopted control strategies for grid-following inverters are discussed in [4], [7], [13]-[14]. When a microgrid is operating in the islanded mode, each DG unit should be able to supply its share of the total load in proportion to its rating. The control strategies for this mode are usually divided into two main types [11], [15] as follows. The first type is communication-based control techniques including concentrated control, master/slave control, and distributed control. These techniques can achieve an excellent voltage regulation and proper power sharing. However, these control strategies which require communication lines between the modules may result in the increased cost of the system. Long distance communication lines will be easier to get interfered, thus reducing the system reliability and expandability. The second type is based on the droop control technique without requiring communications and it is widely used in conventional power systems [2]-[3], [8], [16]-[22]. The reason for the popularity of this droop control technique is that it provides a decentralized control capability that does not depend on external communication links in the control strategy. This technique enables the "plug-and-play" interface and enhances the reliability of the system. However, the communication can be used in addition to the droop control method to enhance the system performance without reducing the reliability [23]-[30].

Traditional droop control techniques have some disadvantages such as slow response to changes of load, inaccuracy in power sharing, unbalanced harmonic current, and dependent on the line impedance of inverters [11]. In addition, difficulties in the power sharing also are due to the reasons as follows:

- The line impedances are not available and different to each others. This affects a lot to the power-sharing due to the different voltage drop. When impedances of the lines connecting inverters to the common connection point are different, the current imbalance will appear as the load sharing error increases [1].
- The heterogeneous line impedance including resistor and capacitance is not suitable for the conventional droop control with pure resistors or pure capacitance applying for the low voltage distribution [1], [22]. Moreover, with the heterogeneous line impedance, the active and reactive power will relate and interact with each other, leading to difficulty for separate control [1].
- As the line impedance changes due to the temperature, the installation position is no

longer making the system more accurate response.

Although the frequency droop technique can achieve an accurate real power sharing, the voltage droop technique typically results in poor reactive power sharing due to the mismatch in the impedances of the DG unit feeders and the different ratings of the DG units [22]-[24]. Consequently, the problem of the reactive power sharing in islanded microgrids has received considerable attention in the literature and many control techniques have been developed to address this issue [31]–[32]. A comprehensive treatment of the concept of virtual impedance to mitigate errors in the reactive power sharing is presented in [23]-[30]. The treatment has focused on the mismatch at the output impedances of the closed-loop controlled inverters that are used to interface the DG units. With a proper design of the voltage controller, the closed-loop output impedances must be negligible at the steady state around the nominal operating frequency. Therefore, the virtual impedance can result in the accurate reactive power sharing. However, the analyses in [23]-[30] did not consider the mismatch in the physical impedance of the feeders, including transformers, cables, and the interface inductors associated with each DG unit.

An interesting droop control strategy has been proposed in [21]. The control strategy is composed of two stages including an initial conventional droop-based control stage and a synchronized compensation stage. The frequency droop is used to control the reactive power sharing and an integral control term is added to the voltage droop to maintain the accuracy of the real power sharing. However, load changes during the compensation period or between the compensation periods may result in a poor power sharing. On the other hand, the analysis and the control strategy introduced in [33] requires that the feeder impedances are resistive. The obtained results from the analysis and control strategy reflect an accurate power sharing if this condition is satisfied. In practice, however, the feeders may have both nonnegligible inductive and resistive components.Therefore, each DG unit should be able to supply in the same rating as analyzed in [34]. If they have different ratings, the strategy will not work. Therefore, the communication network is used as in [35]-[36] to facilitate the estimation of the feeder impedances which are then used to set the virtual impedances to ensure the accurate reactive power sharing. The feeder impedance is estimated at the local DG controller by utilizing the point of common coupling (PCC) where the voltage harmonic data is transferred via a communication link. This is based on the assumption that the phase angle difference between the voltages at the PCC and the inverter output is negligible. This assumption may not hold for long feeders or for higher power levels.

This paper proposes a new method of droop control allowing an accurate load sharing ratio between the paralleled inverters in the islanded microgrids with line impedance estimated online in terms of the conventional resistor. Moreover, the line impedance may vary according to the temperature or frequency at the same time with significant differences between the inverters. The estimation blocks provide the line impedance parameters in the real time line for the proposed droop controller which was built based on the least squares method combined with the Kalman filter. In addition,

secondary control loops are designed to restore the voltage amplitude and frequency of the microgrid by using a combined nominal value SOGI-PLL with generalized integral block and phase lock loop to exactly monitor the voltage magnitude and frequency phase at common PCC. Therefore, the proposed adaptive droop control method can be an alternative one for load sharing control in islanded microgrids.

2. ISLANDED MICROGRID STRUCTURE

Microgrid Structure in Islanded Mode

The structure of an islanded microgrid composes of many inverters connected in parallel. In Figure 1, a block diagram for two inverters is provided.

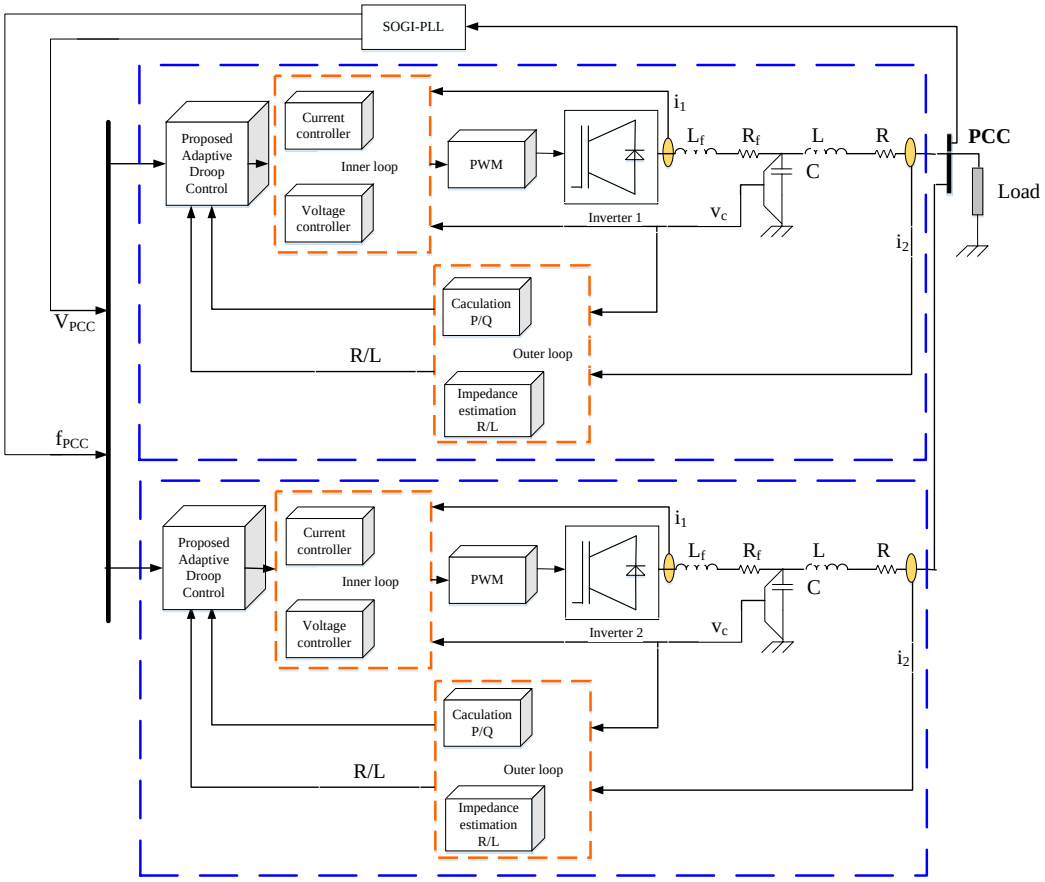

Figure 1. Block diagram of an islanded microgrid.

Each inverter is connected to a common bus at the PCC point through the line impedance, In addition, loads of the microgrid are also connected to the common bus. The droop controller contains two control loops where the outer loop power control divides the capacity of each inverter and the inner loop control makes the voltage and current output of inverter similar to references.The parameter estimation block provides line impedance parameters in real time. The voltage and current signals from the PCC are provided by a low-bandwidth connection. The inner loops are the current and voltage control to adjust the current

and voltage at the inverter output. The SOGI-PLL (Second Order Generalized Integrator - Phase Locked Loop) block is to determine the amplitude and phase angle of the voltage at PCC and support the information for adaptive controller droop.

3. ISLANDED MICROGRID CONTROL

3.1. The proposed droop control

The principle of the droop control method is explained by considering an equivalent circuit of an inverter connected to the AC bus. The analysis method is based on the Thevenin theorem as shown in Figure 2. The active and reactive power supplied by the inverter is calculated as follows:

$$P = \frac{V_S}{R^2 + X^2}\left[R\left(V_S - V_L cos\delta\right) + XV_L sin\delta\right] \quad (1)$$

$$Q = \frac{V_S}{R^2 + X^2}\left[-RV_L sin\delta + X\left(V_S - V_L cos\delta\right)\right] \quad (2)$$

In general, both inductance *X* and resistor *R* are considered. The use of an orthogonal linear rotational transformation matrix T from the active power P and reactive power Q to the active power P' and reactive power Q' is determined by:

$$\begin{bmatrix} P' \\ Q' \end{bmatrix} = [T]\begin{bmatrix} P \\ Q \end{bmatrix} = \begin{bmatrix} \frac{R}{Z}P + \frac{X}{Z}Q \\ -\frac{X}{Z}P + \frac{R}{Z}Q \end{bmatrix}\begin{bmatrix} P \\ Q \end{bmatrix} \quad (3)$$

When the power angle δ is small, equations (1), (2) and (3) can be rewritten as:

$$\delta \cong -\frac{ZQ'}{V_S V_L}; V_S - V_L \cong \frac{ZP'}{V_S} \quad (4)$$

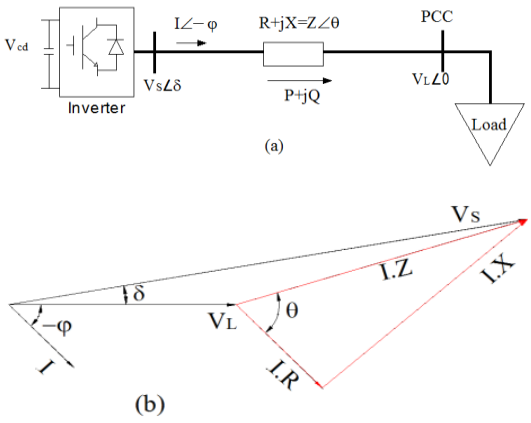

Figure 2. (a) Equivalent schematic of the inverters connected to the load, (b) Vector diagram of voltage and current

From (4), the basis for the well-known frequency and voltage droop regulation through active and reactive power is calculated by:

$$\omega = \omega_0 + m_q Q' \quad (5)$$

$$V_S = V_0 - m_p P' \quad (6)$$

where V_0, ω_0 are the nominal voltage amplitude voltage and frequency of inverter respectively; V_S, ω are the measured amplitude voltage and frequency of inverter, respectively; m_p and m_q are the active and reactive droop coefficients calculated as follows:

$$m_q = \frac{max - min}{Q_{max}}; m_p = \frac{V_{max} - V_{min}}{P_{max}} \quad (7)$$

In the case of impedance of the lines connecting from the inverters to the common PCC is significantly different, the load sharing accuracy is difficult to achieve and the voltage adjustment is also difficult because it depends

on the parameters of the system. From (5) and (6), we will have:

$$m_{q1}Q_1^{'} = m_{q2}Q_2^{'} = \ldots = m_{qn}Q_n^{'} = \Delta\omega_{max} \quad (8)$$

$$m_{p1}P_1^{'} = m_{p2}P_2^{'} = \ldots = m_{pn}P_n^{'} = \Delta V_{max} \quad (9)$$

Combine all equations (1), (2), (3), (5), (6), (8) and (9), we have conditions for the accurately rated power sharing as in (10):

$$\begin{cases} \dfrac{m_{q1}}{Z_1} = \dfrac{m_{q2}}{Z_2} \\ \delta_1 = \delta_2 \\ V_{S1} = V_{S2} \\ \dfrac{m_{p1}}{Z_1} = \dfrac{m_{p2}}{Z_2} \end{cases} \quad (10)$$

To satisfy (10), we must choose the droop coefficients that are proportional to the line impedance. if we adjust the system to meet requirements, the droop will affect the quality of frequency and voltage. Therefore, we have proposed an adaptive controller droop to ensure the accurate power sharing of parallel inverters.

3.1.1 The proposed real power sharing controller

The proposed droop controller still uses the equation in (6) and the voltage of the inverter will be calculated as:

$$V_{S1} = k_{p1}\int\left(V_{S1\_ref} - V_{PCC}\right)dt \quad (11)$$

$$V_{S1\_ref} = V_{01} - m_{p1}P_1^{'} \quad (12)$$

Where k_{p1} is the gain of the integral, V_{PCC} is the voltage at PCC.

From (1), (2) and (3), we can write :

$$P_1^{'} = \frac{V_{S1}^2 - V_{S1}V_{PCC}\cos\left(\delta_1 - \delta_{PCC}\right)}{Z_1} \quad (13)$$

$$Q_1^{'} = -\frac{V_{S1}V_{PCC}\sin\left(\delta_1 - \delta_{PCC}\right)}{Z_1} \quad (14)$$

In equation (13), R_1 and X_1 are the output form the line impedance estimation, V_{PCC} and δ_{PCC} are the output of SOGI-PLL blocks, and δ_1 is the output of the reactive power sharing controller.

Linearize (11), (12) and (13) around $P_1^{'}, V_1, V_{PCC}, \delta_1, \delta_{PCC}$, we will have:

$$\Delta V_{S1} = k_{p1}\int\left(\Delta V_{S1\_ref} - \Delta V_{PCC}\right)dt \quad (15)$$

$$\Delta V_{S1\_ref} = \Delta V_{01} - m_{p1}\Delta P_1^{'} \quad (16)$$

$$\Delta P_1^{'} = A_1\Delta V_{S1} + B_1\Delta V_{PCC} \quad (17)$$

Where:

$$A_1 = \frac{2V_{S1} - V_{PCC}\cos\left(\delta_1 - \delta_{PCC}\right)}{Z_1}$$

$$B_1 = -\frac{V_{S1}}{Z_1}\cos\left(\delta_1 - \delta_{PCC}\right)$$

The relationship among (15), (16) and (17) is shown in Figure 3.

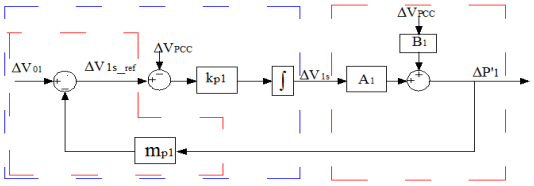

Figure 3. Detail of Small signal adaptive real power sharing droop control.

The transfer function of Figure 3 will be as follows:

$$\Delta P_1^{'}(S)=\frac{k_{p1}A_1}{S+k_{p1}.m_{p1}.A_1}\Delta V_{01}(S)+\frac{SB_1-k_{p1}A_1}{S+k_{p1}.m_{p1}.A_1}\Delta V_{PCC}(S) \quad (18)$$

From (18), we can calculate:

$$\lambda=-k_{p1}.m_{p1}.A_1$$

The transfer function (18) has shown that the constant of loops control can be adjusted by k_{p1}, not by m_{p1}. The real power sharing will not affect the quality of voltage and frequency anymore.

3.1.2 The proposed reactive power sharing controller

The proposed droop controller still uses the equation in (5) while the voltage angle of the inverter will be calculated as:

$$\delta_1=\int\omega_{PCC}dt+k_{q1}\int\left(\omega_{1\_ref}-\omega_{PCC}\right)dt \quad (19)$$

$$\omega_{1\_ref}=\omega_{01}+m_{q1}Q_1^{'} \quad (20)$$

Where k_{p1} is the gain of the integral and ω_{PCC} is the angular frequency at PCC.

In equation (14), R_1 and X_1 are the output from the line impedance estimation, V_{PCC} and δ_{PCC} are the output of SOGI-PLL blocks, V_{1S} is the output of the real power sharing from the controller as mentioned above.

Linearize (14), (19) and (20) around $Q_1^{'},V_{1s},V_{PCC},\delta_1,\delta_{PCC}$, we will have:

$$\omega_1=\omega_{01}+m_{q1}Q_1^{'} \quad (21)$$

$$\Delta\delta_1=\delta_{PCC}+\frac{k_{q1}}{S}\left(\delta_1-\delta_{PCC}\right) \quad (22)$$

$$\Delta Q_1^{'}=C_1\left(\delta_1-\Delta\delta_{PCC}\right) \quad (23)$$

Where: $C_1=-\frac{1}{Z_1}V_{S1}V_{PCC}\cos\left(\delta_1-\delta_{PCC}\right)$

The relationship among (21),(22) and (23) is shown in Figure 4.

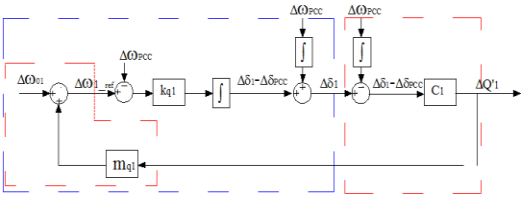

Figure 4. Detail of Small signal adaptive reactive power sharing droop control.

The transfer function in Figure 4 will be as follows:

$$\Delta Q_1^{'}(S)=\frac{k_{q1}C_1}{S-k_{q1}.m_{q1}.C_1}\Delta\omega_{01}(S)-\frac{k_{q1}C_1}{S-k_{q1}.m_{q1}.C_1}\Delta\omega_{PCC}(S) \quad (24)$$

From (24), we calculate $\lambda=k_{q1}.m_{q1}.C_1$

The transfer function (24) has shown that the constant of the loops control can be adjusted by k_{p1}, not by m_{q1}. The real power sharing will not affect the quality of voltage and frequency anymore.

Equations (11) and (19) have shown that when the system achieved the steady-state, the measured voltage of the inverter will be equal to the rated voltage. The proposed droop control has solved the mismatch of power sharing caused by the different impedances of transmission lines. The rated power is always achieved by the controller.

3.2. The line impedance estimation method

3.2.1 The recursive least squares method (LSM)

The equivalent three-phase circuit of the inverter connected to loads is shown in Figure 5.

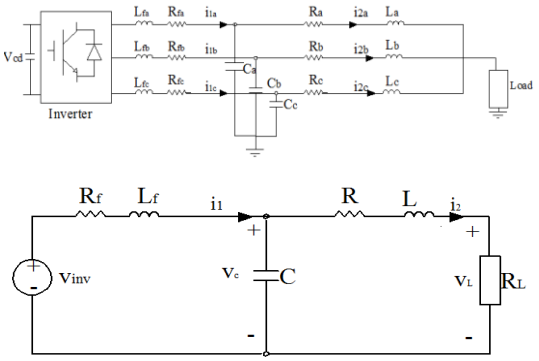

Figure 5. a) The equivalent three-phase circuit of the inverter connected to loads. b) The equivalent single phase circuit of the inverter.

According to the equivalent circuit in Figure 5, we can write as follows:

$$\frac{di_2}{dt} = -\frac{R}{L}i_2 + \frac{1}{L}(v_C - v_L) \qquad (25)$$

Equation (25) can be rewritten as follows:

$$\begin{cases} \dot{X} = AX + Bu \\ Y = CX \end{cases} \qquad (26)$$

where X= $i_2, u = v_C - v_L, A = -\frac{R}{L}, B = \frac{1}{L}$,C=1.

By discretization of the equation (26), we obtain:

$$\begin{cases} i_2(k) = A_d.i_2(k-1) + B_d.u(k-1) \\ y(k) = C_d i_2(k) \end{cases} \qquad (27)$$

The transition matrix is described as follows:

$$\Phi(S) = (SI - A)^{-1} = \left(S + \frac{R}{L}\right)^{-1} = \frac{1}{S + \frac{R}{L}}$$

$$\Phi(t) = e^{-\frac{R}{L}t}, \quad A_d = (T) = e^{-\frac{R}{L}T} \approx 1 - \frac{R}{L}T$$

where T is the sample cycle used to discretize the system.

$$A_d = 1 - \frac{R}{L}T, \; C_d = C = 1$$

$$B_d = \int_0^T (\Phi(\tau)).B.d\tau = \int_0^T e^{-\frac{R}{L}\tau}.\frac{1}{L}d\tau = \frac{T}{L}$$

Equation (27) represents the relationship between the input and output of the object as follows:

$$y(k) = A_d.i_2(k-1) + B_d.u(k-1) + e(k) \quad (28)$$

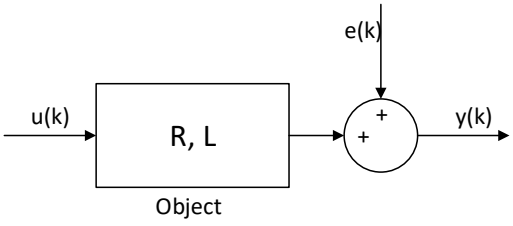

where e(k) is the measurement and process noise.

The relationship between the input and output of (28) can be written as follows:

$$y(k) = \begin{bmatrix} i_2(k-1) \\ u(k-1) \end{bmatrix}^T \begin{bmatrix} A_d \\ B_d \end{bmatrix} = \varphi(k)^T.\theta + e(k)$$

$$(29)$$

where φ(k) is the regression vector containing the variables and sample data of voltage and current.

$$\theta = \begin{bmatrix} A_d \\ B_d \end{bmatrix} = \begin{bmatrix} 1-\frac{R}{L}T \\ \frac{T}{L} \end{bmatrix} = \begin{bmatrix} \theta_1 \\ \theta_2 \end{bmatrix} \qquad (30)$$

The problem is to estimate the parameters of vector θ based on the current data and voltage. Neglecting the noise e(k), we have predicted the linear regression:

$$\hat{y}(k,\theta) = \varphi(k)^T.\theta$$

The store of all the sample data in the real time and calculation of the volume do not increase much time due to using the recursive least squares method. This algorithm includes the equation as follows:

$$\begin{cases} \hat{\theta}(k) = \hat{\theta}(k-1) + L(k).\varepsilon(k) \\ \varepsilon(k) = y(k) - \varphi(k)^T.\hat{\theta}(k-1) \\ L(k) = \dfrac{P(k-1)\varphi(k)}{\lambda + \varphi(k)^T.P(k-1).\varphi(k)} \\ P(k) = \dfrac{1}{\lambda}[P(k-1) - \dfrac{P(k-1).\varphi(k).\varphi(k)^T.P(k-1)}{\lambda + \varphi(k)^T.P(k-1).\varphi(k)} \end{cases} \qquad (31)$$

where λ is the forget coefficient selected in the range from 0.98 to 0.995.

The line impedance is estimated by a technique based on the recursive least squares method (LSM). The parameter vector θ_{LSM} determined from the measured chain value should be affected by the noise or error in equation (31). Therefore, we use the Kalman filter to filter out the noise and obtain the value of θ_{Kalman} approximate with the real value.

3.2.2 Using the Kalman filter algorithm to filter noise for θ

The Kalman filter is to estimate a process by using a form of the feedback control. The process of the Kalman filter is shown in Figure 6. The Kalman filter firstly estimates the state of the process at a time and then gets the feedback from the measured value to correct the estimation. Therefore, the equation of the Kalman filter is composed of two groups including the time update group and measurement update group.

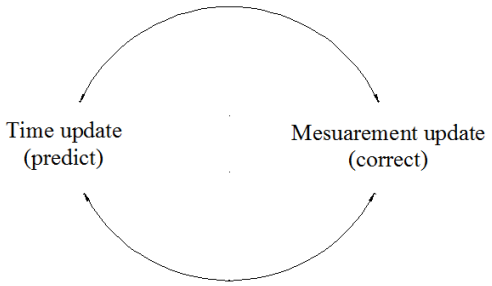

Figure 6. Process of Kalman filter.

The equations for the updated time are to predict the state:

$$\begin{cases} \theta_{pred}(k) = A.\theta_{est}(k-1) & (32) \\ P_{pred}(k) = A.P_{est}(k-1).A^T + Q & (33) \end{cases}$$

The equations for measurement updated to correct estimation:

$$\begin{cases} K(k) = P_{pred}(k).H^T.\left(H.P_{pred}(k).H^T + R\right)^{-1} & (34) \\ \theta_{est}(k) = \theta_{pred}(k) + K(k).\left(\theta(k) - H.\theta_{pred}(k)\right) & (35) \\ P_{est}(k) = \left(I - K(k).H\right).P_{pred}(k) & (36) \end{cases}$$

where K is the Kalman gain.

$$A=\begin{bmatrix}1 & 0\\ 0 & 1\end{bmatrix},\ B=0,\ H=\begin{bmatrix}1 & 0\\ 0 & 1\end{bmatrix},\ I=\begin{bmatrix}1 & 0\\ 0 & 1\end{bmatrix}$$

The start of Kalman filter algorithm is initialized at the initial values:

$$\theta_{est}(k-1)=\begin{bmatrix}0\\ 0\end{bmatrix}, P_{est}(k-1)=\begin{bmatrix}1 & 0\\ 0 & 1\end{bmatrix}$$

$$Q=\begin{bmatrix}0.001 & 0\\ 0 & 0.001\end{bmatrix}, R=\begin{bmatrix}0.00025 & 0\\ 0 & 0.00025\end{bmatrix}$$

Equations (34)-(36) are applied to the Kalman filter and the procedure is repeated until the difference between the actual value and the value estimated less than a predetermined error ε. The result at the output of the Kalman filter is a vector $\theta_{Kalman}=\theta_{est}$ determined by:

$$\theta_{Kalman}=\begin{bmatrix}\theta_{1\_Kalman}\\ \theta_{2\_Kalman}\end{bmatrix}=\begin{bmatrix}1-\dfrac{R_{Kalman}}{L_{Kalman}}*T\\ \dfrac{T}{L_{Kalman}}\end{bmatrix} \quad (37)$$

From (37), we obtain the value of R_{Kalman}, L_{Kalman}.

3.3. Model of single phase SOGI-PLL

Figure 7 shows the structure of the SOGI-PLL. Both the adaptive filtering technique and in-quadrature phase detection technique are used in the SOGI-PLL to generate the frequency and phase outputs. This system has a double feedback loop, i.e. the frequency/phase generator provides both the phase-angle to the Park transform and the central frequency to the SOGI-QSG (Second Order Generalized Integrator - Quadrature Signal Generation).

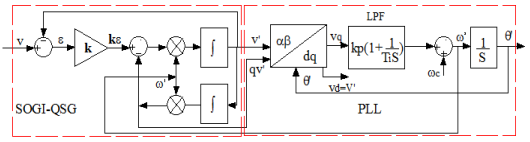

Figure 7. Model of single phase SOGI-PLL.

The parameters of SOGI-PLL are chosen as follows: $k=\sqrt{2}$, t_s=100ms, $\varepsilon=\dfrac{1}{\sqrt{2}}$, $T_i=\dfrac{t_s.\varepsilon^2}{2.3}=0.021s$

Figure 8 shows the responses of the SOGI-PLL.

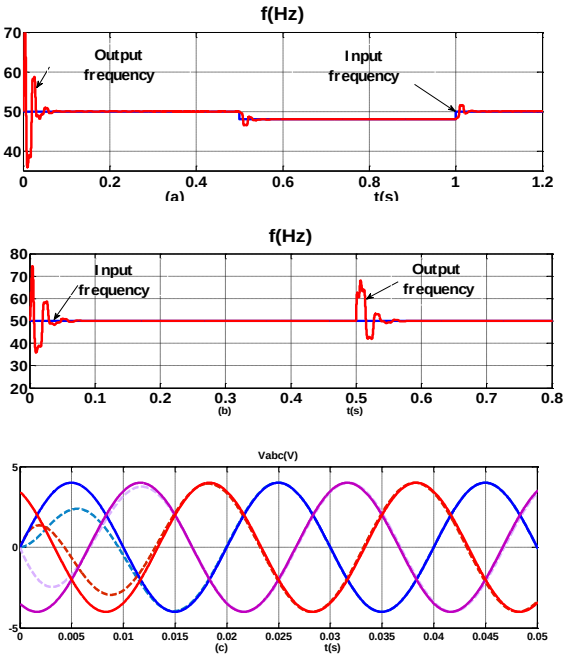

Figure 8. The responses of the SOGI-PLL.

Figure 8a shows the frequency response of the SOGI-PLL when the frequency of the input signal changes from 50Hz to 48Hz at t = 0.5s and from 48Hz to 50Hz at t = 1s. Figure 8b shows the frequency response of the SOGI-PLL when the phase angle of the input signal changes

from 0^o to 45^o at t = 0.5s. Figure 8c shows the response of the input and output voltages of the SOGI-PLL. The simulation results in Figure 8 have shown that SOGI-PLL can exactly obtain the voltage amplitude and frequency at the point of common coupling (PCC). They will be the input for inner-controller. So when we have more exact values, we will get more accurate power sharing.

4. SIMULATION RESULTS AND DISCUSSION

A microgrid with two parallel DG units as in Figure 1 is simulated in Matlab/Simulink. All the simulation parameters of the system are given in Table 1.

Table 1. Parameters for the controllers

Parameters	Value
Input source voltage V_{cd} (V)	600
Filter inductance L_f (mH)	1.2
Filter resistance R_f (Ω)	0.2
Filter capacitance C (μF)	50
Switching frequency f_0 (kHz)	10
Rate frequency f_0 (Hz)	50
Rate power (kVA)	5
Rate voltage $V_{AC,\,p}$ (V)	310
Droop coefficient m_q (rad/s/Var)	2.5e-4
Droop coefficient m_p (V/W)	1.7e-3

4.1. Line parameters change with fixed load.

In this simulation, the line parameters of two inverters are provided in Table 2. The results from the simulation are given in Figure 9.

Table 2. Line Parameters of two inverters

Line parameters	Inverter 1		Inverter 2	
Resistance R(Ω)	t = 0-3s	0.8	t = 0-3s	1
	t = 3-6s	0.4	t = 3-6s	0.5
	t = 6-9s	0.6	t = 6-9s	0.7
Inductance L(mH)	t = 0-3s	0.8	t = 0-3s	1
	t = 3-6s	0.4	t = 3-6s	0.5
	t = 6-9s	0.6	t = 6-9s	0.7

Figures 9a and 9b have shown the performance of proposed strategy when the line parameters change. Figure 9c and 9d show the performance of conventional droop control. When the line parameters change at 3s and 6s, both strategies have normal real power sharing but the conventional droop control can't achieve accuracy reactive power sharing because of the mismatch in line impedances. Only the proposed strategy with line impedance estimation block (Figure 9e, 9f) can share accurate real and reactive power in 1:1 ratio. The voltage drop is always in the limit (Figure 9g).

4.2. Line parameters and loads change with the same power sharing ratio.

The line parameters of two inverters for this simulation are provided in Table 3. The obtained simulation results are given in Figure 10.

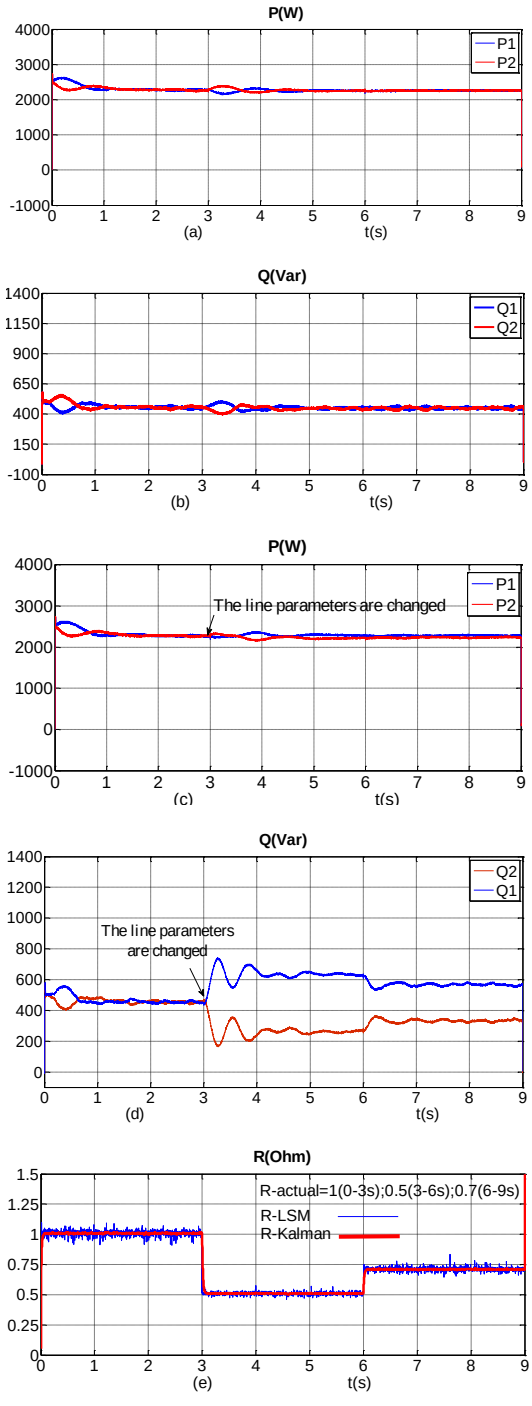

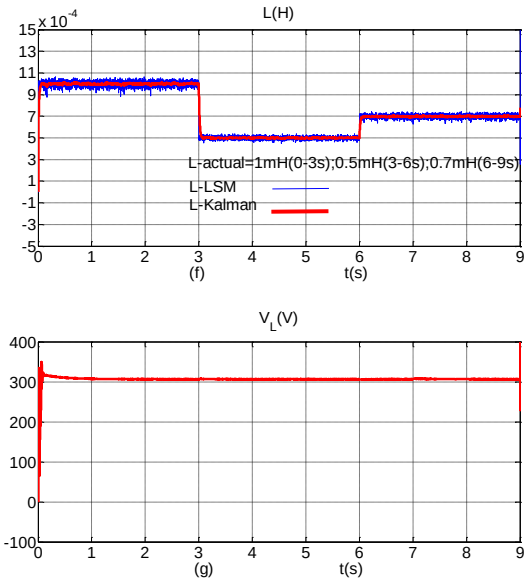

Figure 9. (a) Real power with the line impedance estimate, (c) Real power without the line impedance estimate; (b) Reactive power with the line impedance estimate, (d) Reactive power without the line impedance estimate; (e) Resistance estimation; (f) Inductance estimation; (g) Load voltage.

Table 3. Line Parameters of two inverters

Line parameters	Inverter 1		Inverter 2	
Resistance R(Ω)	t = 0-3s	0.8	t = 0-3s	1
	t = 3-6s	0.4	t = 3-6s	0.5
	t = 6-9s	0.6	t = 6-9s	0.7
Inductance L(mH)	t = 0-3s	0.8	t = 0-3s	1
	t = 3-6s	0.4	t = 3-6s	0.5
	t = 6-9s	0.6	t = 6-9s	0.7

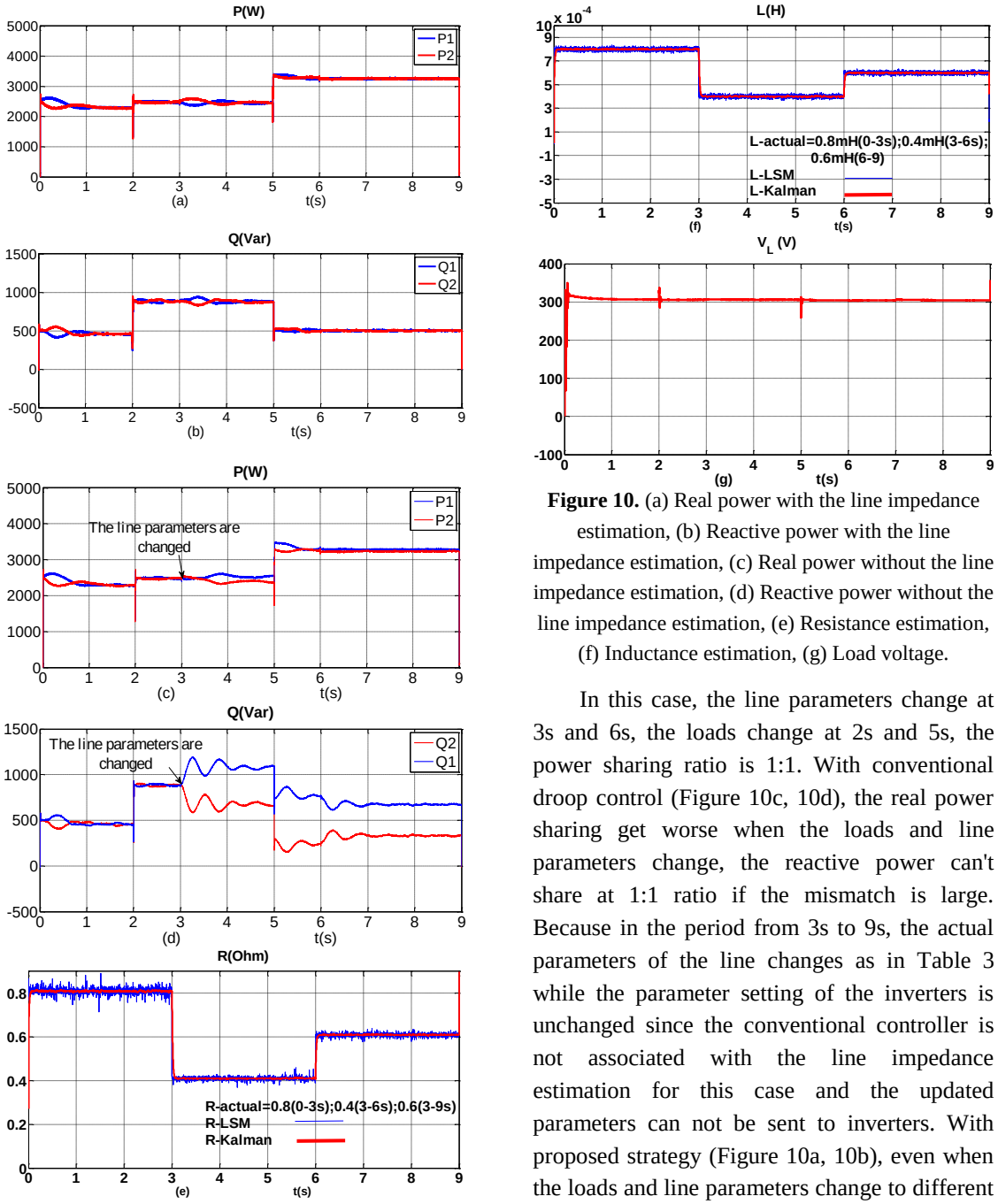

Figure 10. (a) Real power with the line impedance estimation, (b) Reactive power with the line impedance estimation, (c) Real power without the line impedance estimation, (d) Reactive power without the line impedance estimation, (e) Resistance estimation, (f) Inductance estimation, (g) Load voltage.

In this case, the line parameters change at 3s and 6s, the loads change at 2s and 5s, the power sharing ratio is 1:1. With conventional droop control (Figure 10c, 10d), the real power sharing get worse when the loads and line parameters change, the reactive power can't share at 1:1 ratio if the mismatch is large. Because in the period from 3s to 9s, the actual parameters of the line changes as in Table 3 while the parameter setting of the inverters is unchanged since the conventional controller is not associated with the line impedance estimation for this case and the updated parameters can not be sent to inverters. With proposed strategy (Figure 10a, 10b), even when the loads and line parameters change to different values, the real and reactive power sharing are still good with line impedance estimation. In figure 10e and 10f, the estimation block can instantly give new values when line parameters change with high accuracy. This result has demonstrated its usefulness.

4.3. Line parameters and loads change with the different power sharing ratio.

In this case, the rated power ratio of the inverters is 1:2 and the line parameters of the two inverters are provided as in Table 4. The obtained results from the simulation are given in Figure 11.

Table 4. Line Parameters of two inverters

Line parameters	Inverter 1		Inverter 2	
Resistance R(Ω)	t = 0-3s	1	t = 0-3s	1
	t = 3-6s	0.4	t = 3-6s	0.8
	t = 6-9s	0.5	t = 6-9s	1
Inductance L(mH)	t = 0-3s	1	t = 0-3s	1
	t = 3-6s	0.4	t = 3-6s	0.8
	t = 6-9s	0.5	t = 6-9s	1

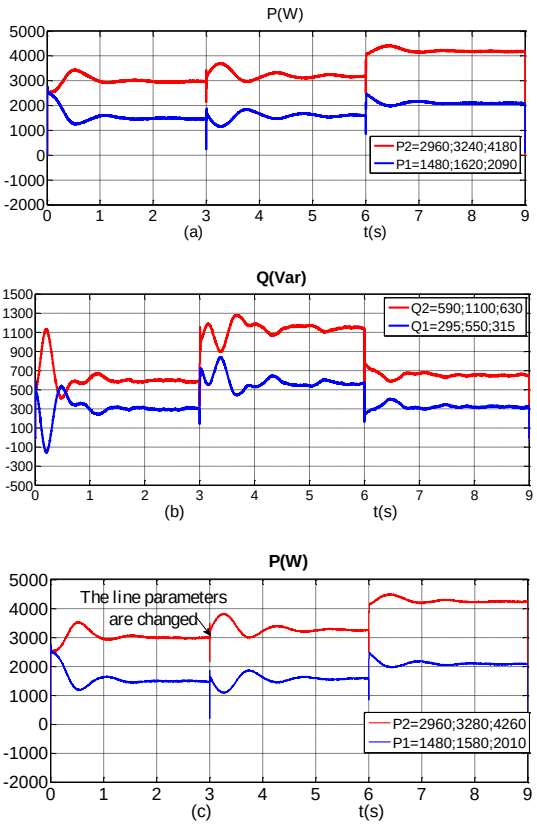

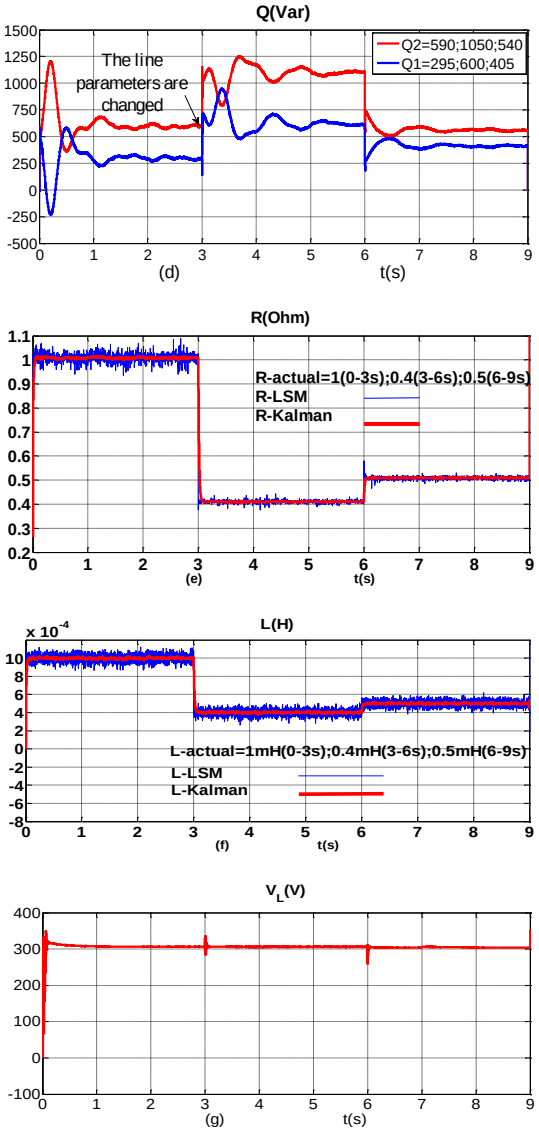

Figure 11. (a) Real power with the line impedance estimation, (b) Reactive power with the line impedance estimation, (c) Real power without the line impedance estimate, (d) Reactive power without the line impedance estimation, (e) Resistance estimation, (f) Inductance estimation, (g) Load voltage.

In this case, the line parameters change at 3s and 6s, the loads change at 2s and 5s, the power sharing ratio will changes to 1:2 not 1:1 like case 4.3. With conventional droop control (Figure 11c, 11d), the power sharing

performances are worse than upper case because of the ratio change and mismatch in line impedance. After 6s, control errors go up to 50% when we have Q1=405Var and Q2=540Var. The ratio at the moment is not 1:2. With proposed strategy (Figure 11a, 11b), even when the loads and line parameters change to different values, the performances of power sharing have ensured with low errors control and small overshoot. In figure 11e and 11f, the estimation block can instantly give new values when line parameters change with high accuracy. The result of proposed droop control with estimation block is very positive.

4.4. Hardware Implementation Using DSP 28335.

The research has been also implemented on a practical model developed in our laboratory. The experiment model in the laboratory has three 3-phase inverters and a driver of Semikron, LEM HX 20P and a LV–25P plays the role as a voltage and current sensor. The experimental apparatus in the laboratory for the research are shown Figure 12. The proposed control algorithm has been implemented on the TMS320F28335 DSP controller and the test results have been captured by Tektronix TDS2014B oscilloscope and Fluke 345 PQ clamp meter. To maintain the power demand of loads, the three inverters are used with paralleled output connections while RS485 lines are responsibility for the communication network. For the hardware implementation, two test cases are considered including the ratio of the active and reactive power of 1:1:1 with loads change on time corresponding to Mode 1 on. The experimental results have verified the advantages of the proposed control algorithm through three case studies.

4.5. Case study 1: P_1:P_2:P_3 = 1:1:1, Q_1:Q_2:Q_3 = 1:1:1, Load fixed at a pre-determined value.

For this case, the ratio of active and reactive power is 1:1:1 for the three inverters with the load fixed at a pre-determined value. The measured active power outputs for the three inverters are shown in Figure 13. The obtained active power for the three inverters are P_1 = 945 W, P_2 = 935 W, P_3 = 945 W. The real power sharing errors, in this case, are very small.

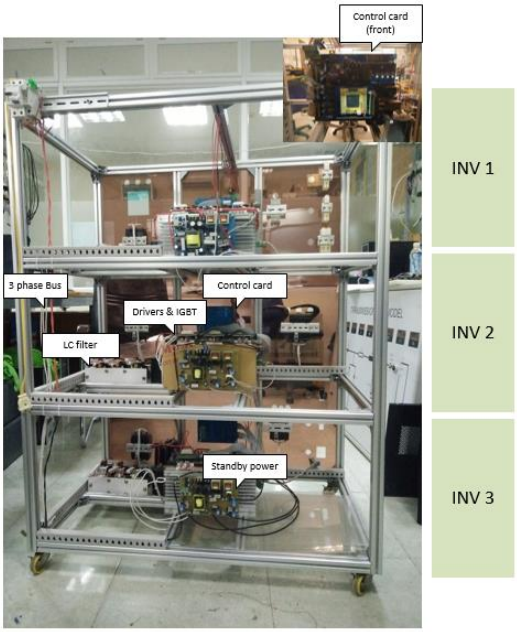

Figure 12. Experimental apparatus in laboratory.

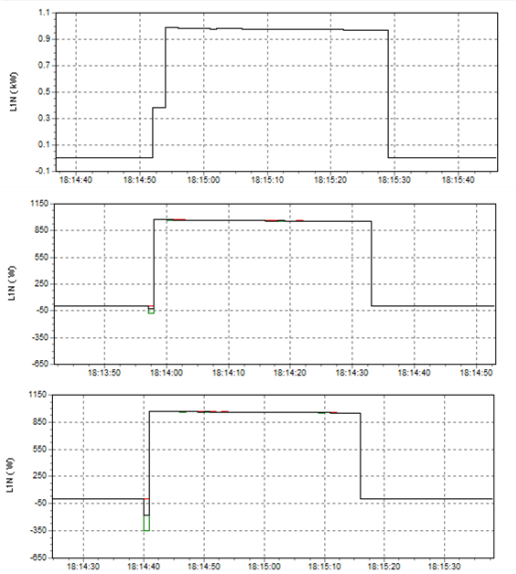

Figure 13. The active power of the three inverters for Case study 1 of hardware experiment.

4.6. Case study 2: P_1:P_2:P_3 = 1:1:1, Q_1:Q_2:Q_3 = 1:1:1, Load changes with steps within the pre-determined limits.

This case is corresponding to the ratio of active and reactive power still being 1:1:1 and the load changes with steps within the pre-determined limits. The measured active power outputs for the three inverters are shown in Figure 14. The obtained active power for the three inverters rises in the limits as P_1max = 2025 W, P_2max = 2045 W, P_3max = 2025 W, P_1min = 100 W, P_2min = 125 W, P_3min = 125 W. These results have demonstrated the system's response when the load continuously changing on time while keeping constant ratio.

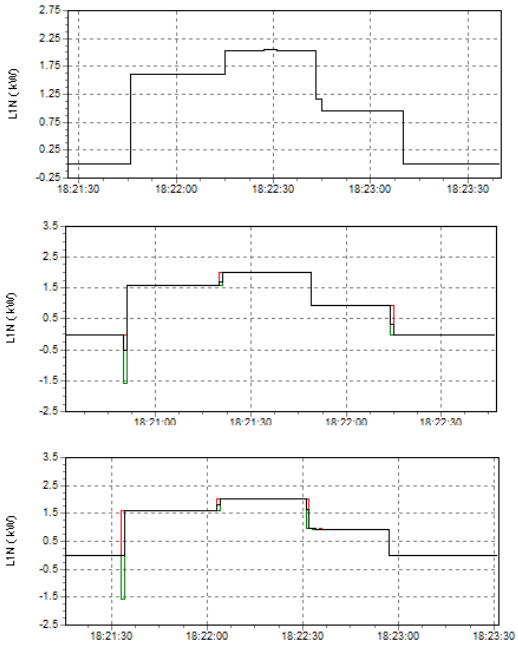

Figure 14. The active power of the three inverters for Case study 2 of hardware experiment

4.7. Conclusion

This paper proposes a new method of droop control allowing an accurate load sharing ratio between the paralleled inverters in the islanded microgrids with line impedance estimated online in terms of the conventional resistor. Moreover, the line impedance may vary according to the temperature or frequency at the same time with significant differences between the inverters. The estimation blocks will provide the line impedance parameters in the real time line for the proposed droop controller which was built based on the least squares method combined with the Kalman filter. Even while line impedances and loads change at the same time, the refresh rate is fast enough to keep system stability and high accuracy power sharing. The results in Matlab Simulink and hardware implementation have demonstrated the

superiority of proposed strategy in any case with any ratio.

Acknowledgment: *This research is funded by Vietnam National University Ho Chi Minh City (VNU-HCM) under grant number B2014-20-06.*

Điều khiển Droop thích nghi các bộ nghịch lưu kết nối song song kết hợp ước lượng tổng trở đường dây

- **Lê Minh Phương**
- **Phạm Thị Xuân Hoa**
- **Hoàng Võ Đức Duy**
- **Nguyễn Minh Huy**

Trường Đại học Bách Khoa, ĐHQG-HCM

TÓM TẮT

Bài báo trình bày kỹ thuật điều khiển mới chia tải cho các bộ nghịch lưu ba pha kết nối song song trong lưới siêu nhỏ độc lập với khả năng ước lượng được trở kháng đường dây bằng bộ lọc Kalman. Khi mà trở kháng đường dây bị thay đổi liên tục do ảnh hưởng của tần số và nhiệt độ môi trường, khả năng đáp ứng nhanh của các bộ nghịch lưu bị giảm xuống. Vì vậy, bài báo này sẽ trình bày kỹ thuật điều khiển Droop mới có thể hoạt động với nhiều trở kháng đường dây khác nhau, trong điều kiện thuần trở R và thuần kháng X. Sử dụng phương pháp bình phương cực tiểu kết hợp với bộ lọc Kalman, phương pháp ước lượng này cho kết quả khả thi trong trường hợp trở kháng thay đổi liên tục. Ngoài ra một vòng lặp thứ hai được thiết kế để phục hồi điện áp và dòng điện sau Droop, bằng bộ khóa pha và bộ SOGI-PLL bám sát được điện áp và tần số điểm kết nối chung PCC. Mô hình điều khiển đã được mô phỏng trên Matlab/Simulink với ba bộ nghịch lưu song song có tỷ lệ công suất giữa các bộ nghịch lưu khác biệt. Kết quả mô phỏng thể hiện được độ chính xác cao của kỹ thuật điều khiển đề xuất. Vì vậy, phương pháp điều khiển Droop thích nghi dựa trên ước lượng trở kháng đường dây có thể ứng dụng tốt chia sẻ tải trong một lưới siêu nhỏ độc lập.

Từ khoá: *Các bộ nghịch lưu song song, điều khiển Droop, ước lượng tổng trở đường dây, bộ lọc Kalman*

REFERENCES

[1]. Hua Han, Xiaochao Hou, Jian Yang , Jifa Wu, Mei Su, and Josep M. Guerrero *"Review of Power Sharing Control Strategies for Islanding Operation of AC Microgrids,"* IEEE Trans. Smart Grid, vol. 7, no. 1, pp. 200–216, Jan. 2016.

[2]. K. Moslehi and R. Kumar, *"A reliability perspective of the smart grid,"* IEEE Trans. Smart Grid, vol. 1, no. 1, pp. 57–64, Jun. 2010.

[3]. R. H. Lasseter, *"Microgrids,"* in Proc. IEEE Power Eng. Soc. Winter Meeting, New York, NY, USA, 2002, pp. 305–308.

[4]. R. H. Lasseter and P. Paigi, *"Microgrid: A conceptual solution,"* in Proc. IEEE Power Electron. Spec. Conf., Aachen, Germany, 2004, pp. 4285–4290.

[5]. J. Rocabert, A. Luna, F. Blaabjerg, and P. Rodriguez, *"Control of power converters in AC microgrids,"* IEEE Trans. Power Electron., vol. 27, no. 11, pp. 4734–4739, Nov. 2012.

[6]. A. Molderink, V. Bakker, M. G. C. Bosman, J. L. Hurink, and G. J. M. Smit, *"Management and control of domestic smart grid technology,"* IEEE Trans. Smart Grid, vol. 1, no. 2, pp. 109–119, Sep. 2010

[7]. F. Blaabjerg, R. Teodorescu, M. Liserre, and A. V. Timbus, *"Overview of control and grid synchronization for distributed power generation systems,"* IEEE Trans. Ind. Electron., vol. 53, no. 5, pp. 1398–1409, Oct. 2006.

[8]. Q.-C. Zhong. "Robust Droop Controller for Accurate Proportional Load Sharing Among Inverters Operated in Parallel". IEEE Trans. Power Electron vol. 60, no. 4, pp. 1281–1291, April. 2013.

[9]. R. Lasseter, *"Microgrids,"* inProc. IEEE Power Eng. Soc. Winter Meeting, 2002, vol. 1, pp. 305–308.

[10]. G. Weiss, Q.-C. Zhong, T. C. Green, and J. Liang. (2004, Jan.). *"H∞ repetitive control of DC-AC converters in microgrids"*. IEEE Trans. Power Electron.[Online]. 19(1), pp. 219–230.

[11]. J. Guerrero, J. Vasquez, J. Matas, M. Castilla, and L. García de Vicuña, *"Control strategy for flexible microgrid based on parallel line-interactive UPS systems,"* IEEE Trans. Ind. Electron., vol. 56, no. 3, pp. 726–736, Mar. 2009.

[12]. S. V. Iyer, M. N. Belur, and M. C. Chandorkar, *"A generalized computational method to determine stability of a multi-inverter microgrid,"* IEEE Trans. Power Electron., vol. 25, no. 9, pp. 2420–2432, Sep. 2010.

[13].. J. Justo, F. Mwasilu, and J. Lee, *"AC microgrids versus DC microgrids with distributed energy resources: A review,"* Renew. Sustain. Energy Rev., vol. 24, pp. 387–405, Aug. 2013.

[14]. M. A. Eltawil and Z. Zhao, *"Grid-connected photovoltaic power systems: Technical and potential problems—A review,"* Renew. Sustain. Energy Rev., vol. 14, no. 1, pp. 112–129, Jan. 2010.

[15]. J. Guerrero, L. García de Vicuña, J. Matas, M. Castilla, and J. Miret, *"Output impedance design of parallel-connected UPS inverters with wireless load-sharing*

control," IEEE Trans. Ind. Electron., vol. 52, no. 4, pp. 1126–1135, Aug. 2005.

[16]. P. Piagi and R. H. Lasseter, *"Autonomous control of microgrids,"* in Proc. Power Eng. Soc. Gen. Meeting, Montreal, QC, Canada, 2006, pp. 8–15.

[17]. M. C. Chandorkar, D. M. Divan, and R. Adapa, *"Control of parallel connected inverters in standalone AC supply systems,"* IEEE Trans. Ind. Appl., vol. 29, no. 1, pp. 136–143, Jan. 1993.

[18]. J. M. Guerrero, J. C. Vasquez, and J. Matas, *"Control strategy for flexible microgrid based on parallel line-interactive UPS systems,"* IEEE Trans. Ind. Electron., vol. 56, no. 3, pp. 726–736, Mar. 2009.

[19]. J. Hu, J. Zhu, D. G. Dorrell, and J. M. Guerrero, *"Virtual flux droop method—A new control strategy of inverters in microgrids,"* IEEE Trans. Power Electron., vol. 29, no. 9, pp. 4704–4711, Sep. 2014.

[20]. L. Y. Lu and C. C. Chu, "Consensus-based droop control synthesis for multiple DICs in isolated micro-grids," IEEE Trans. Power Syst., to be published.

[21]. J. He and Y. W. Li, *"An enhanced microgrid load demand sharing strategy,"* IEEE Trans. Power Electron., vol. 27, no. 9, pp. 3984–3995, Sep. 2012.

[22]. W. Yao, M. Chen, and J. Matas, "Design and analysis of the droop control method for parallel inverters considering the impact of the complex impedance on the power sharing," IEEE Trans. Ind. Electron., vol. 58,no. 2, pp. 576–588, Feb. 2011.

[23]. Hisham Mahmood, Dennis Michaelson, and Jin Jiang *"Accurate Reactive Power Sharing in an Islanded Microgrid Using Adaptive Virtual Impedances,"* IEEE Power Electronics, vol. 30, no. 3, pp. 1605–1618, March. 2015.

[24]. J. M. Guerrero, M. Chandorkar, T.-L. Lee, and P. C. Loh, *"Advanced control architecture for intelligent microgrids—Part I: Decentralized and hierarchical control,"* IEEE Trans. Power Electron., vol. 60, no. 4, pp. 1254–1262, Apr. 2013.

[25]. Josep M. Guerrero; Juan C. Vasquez; José Matas; Luis García de Vicuna; Miguel Castilla*, "Hierarchical control of droop-controlled ac and dc microgrids—A general approach towards standardization,"* IEEE Trans. Ind. Electron., vol. 58, no. 1, pp. 158–172, Jan. 2011.

[26]. M. N. Marwali, J.-W. Jung, and A. Keyhani, *"Control of distributed generation systems—Part II: Load sharing control,"* IEEE Trans. Power Electron., vol. 19, no. 6, pp. 1551–1561, Nov. 2004.

[27]. J. C. Vasquez, J. M. Guerrero, M. Savaghebi, J. Eloy-Garcia, and R. Teodorescu, *"Modeling, analysis, and design of stationary-reference frame droop-controlled parallel three-phase voltage source inverters,"* IEEE Trans. Ind. Electron., vol. 60, no. 4, pp. 1271–1280, Apr. 2013.

[28]. M. Savaghebi, A. Jalilian, J. C. Vasquez, and J. M. Guerrero, *"Secondary control scheme for voltage unbalanced compensation in an islanded droop*

controlled microgrid," IEEE Trans. Smart Grid, vol. 3, no. 2, pp. 797–807, Jun. 2012.

[29].M Savaghebi, A. Jalilian, J. C. Vasquez, and J. M. Guerrero, *"Secondary control for voltage quality enhancement in microgrids,"* IEEE Trans. Smart Grid, vol. 3, no. 4, pp. 1893–1902, Dec. 2012.

[30].M. A. Abusara, J. M. Guerrero, and S. M. Sharkh, *"Line-interactive ups for microgrids,"* IEEE Trans. Ind. Electron., vol. 61, no. 3, pp. 1292–1300, Mar. 2014.

[31].Juan C. Vasquez, Josep M. Guerrero, Alvaro Luna, Pedro Rodríguez, and Remus Teodorescu *"Adaptive Droop Control Applied to Voltage-SourceInverters Operating in Grid-Connected and Islanded Modes"* IEEE Trans.on industrial Electronics., vol. 56, no. 10, pp. 4088–4098, Octorber 2009.

[32].D. De and V. Ramanarayanan, *"Decentralized parallel operation of inverters sharing unbalanced and nonlinear loads,"* IEEE Trans. Power Electron., vol. 25, no. 12, pp. 3015–3025, Dec. 2010.

[33].Y. W. Li and C.-N. Kao, "An accurate power control strategy for power-electronics-interfaced distributed generation units operating in a low-voltage multibus microgrid," IEEE Trans. Power Electron., vol. 24, no. 12, pp. 2977–2988, Dec. 2009.

[34].H. Mahmood, D. Michaelson, and J. Jiang, *"Accurate reactive power sharing in an islanded microgrid using adaptive virtual impedances,"* IEEE Trans. Power Electron., vol. 30, no. 3, pp. 1605–1617, Oct. 2014

[35].J. He, Y. W. Li, J. M. Guerrero, J. C. Vasquez, and F. Blaabjerg, *"An islanded microgrid reactive power sharing scheme enhanced by programmed virtual impedances,"* inProc. IEEE Int. Symp. Power Electron. Distrib. Gener. Syst., Aalborg, Denmark, 2012, pp. 229–235.

[36].J. He, Y. W. Li, J. M. Guerrero, F. Blaabjerg, and J. C. Vasquez, *"An islanding microgrid power sharing approach using enhanced virtual impedance control scheme,"* IEEE Trans. Power Electron., vol. 28, no. 11, pp. 5272–5282, Nov. 2013.